FY-13 FCRD Milestone M3FT-13OR0202311 Weldability of ORNL Accident Tolerant Fuel Cladding Model Alloys For Thin Walled Tubes

K.G. Field, M.N. Gussev, and Y. Yamamoto

Abstract

Ferritic FeCrAl-based alloys show increased oxidation resistance for accident tolerant applications as fuel cladding. This study focuses on investigating the weldability of three model FeCrAl alloys with varying alloy compositions using laser-welding techniques. A detailed study of the mechanical properties of bead-on-plate welds was used to determine the quality of welds as a function of alloy composition. Laser welding resulted in defect free welds devoid of cracking or inclusions. Initial results indicate a reduction in the yield strength of weldments compared to the base material due to distinct changes in the microstructure within the fusion zone. Although a loss of yield strength was observed, there was no significant difference in the magnitude of the tensile property changes with varying Cr or Al content. Also, there was no evidence of embrittlement; the material in the fusion zones demonstrated ductile behavior with high local ductility.

1. Introduction

A critical aspect of fuel rod performance is the integrity of the fuel rod end cap weld. Typical fuel elements utilize a circumferential weld in either a butt weld or corner weld configuration to seal the fuel rod during final assembly. Small amounts of contamination or weld defects such as pore formation can lead to costly fuel failures [1]. FeCrAl alloys are being explored for their enhanced accident tolerance compared to the industry standard zirconium alloys [2-4]. This report describes the preliminary investigation of the quality of weldments made in three model alloys of FeCrAl with Y additions. Laser-welding techniques were utilized as the large heat input in a small region results in reduced microstructural changes in the heat-affected zone. Furthermore, laser welding has been utilized by industry for fuel rod fabrication [1]. Microstructural characterization and mechanical testing of full penetration, bead-on-plate welds were used to evaluate the weldability of the candidate alloys.

2. Experimental Procedure

2.1 Sample Preparation

Three model FeCrAlY ferritic alloys with designations B125Y, B154Y-2 and B183Y-2 were used in this study. The composition of each alloy is provided in Table 1. The wide range of Cr and Al contents was selected to investigate alloying effects and to determine if there was an upper or lower threshold for weldability of FeCrAlY alloys. Starting material was heat-treated and hot forged/rolled to control grain size to 20-50 μm, followed by 10% cold rolling to flatten the product. The resulting sheet stock with a nominal thickness of 800 μm was used in this study. Samples for welding were wire brushed to remove any surface oxides or contamination from the material processing steps before loading into the welding apparatus.

Table 1: Composition (wt. %) of FeCrAlY candidate alloys

Alloy	Fe	Cr	Al	Y
B125Y	Bal.	11.96	4.42	0.027
B154Y-2	Bal.	15.03	3.92	0.035
B183Y-2	Bal.	17.51	2.93	0.017

2.2 Laser Welding Parameters

A pulsed laser-welding machine was used. The specimens were held in the holder of the laser-welder to perform autogenous welding. Welding was completed using a 102 mm focusing lens, with weld parameters: pulse length 7 ms, 25 pulses per second, and 178 mm/min welding speed in an inert argon cover gas. Linear welds were conducted parallel to the traverse direction on each specimen. Figure 1 shows representative optical micrographs of topside and backside weldments on the B154Y alloy. Post weld inspection shows no signs of cracking, porosity, or other detrimental defects in the fusion zone or heat affected zone (HAZ) of the specimens.

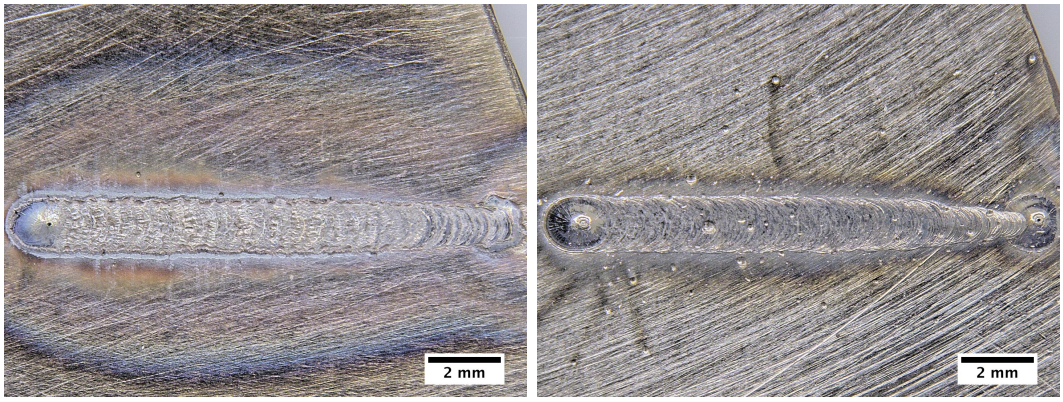

Figure 1: Optical micrograph showing the traverse laser weld incident surface (left) and exit surface (right) in the B154Y-2 alloy. Optical inspection shows no cracking or surface defects in the specimen.

2.3 Metallography and Microhardness Traverses

Weld specimens were cross-sectioned using a low speed diamond saw and polished to a mirror finish using standard metallographic procedures. Polished cross section specimens were etched to reveal grain structure in the base, HAZ, and weld metal. Etched specimens were imaged using an Am Scope NMM-800RF/TRF optical microscope. Average grain diameter was calculated using the linear mean intercept method described in ASTM E112-12.

Hardness traverses across the weld cross sections used a Wilson Model 402MVD Vickers Microhardness tester. The indent load was 300 g with a dwell time of 15 s. Indent spacing was maintained at 0.2 mm. Hardness tests were performed ± 2.6 mm from the centerline of each weld, which roughly corresponds to the gauge length of the sub-sized tensile specimens, described in the following section. Indent diagonals were measured manually since low contrast between indent and surface prevented

utilization of automated routines.

2.4 Mechanical Testing

Sub-sized tensile specimens were machined from the welded and non-welded sheet specimens where welded specimens had the fusion zone orientated perpendicular to the load direction. The cross-weld specimen dimensions and location of the fusion zone within the specimen is shown in Figure 2. Sub-sized specimens were utilized to maximize data from the limited volume of material provided for the study. Specimens were manufactured using electro-discharge machining (EDM). Care was taken to center the fusion zone in the gauge length of the specimen, but some deviation from the ideal position occurred. At least two specimens were machined from each weld traverse to eliminate outliers from the analysis. Specimens were imaged optically after machining to locate the fusion zone within the gauge length, as shown in the example in Figure 2. Care was taken to document the weld direction and extracted specimen location. Specimens were ground using 1200 grit SiC paper to provide a uniform thickness along the gauge length and remove any extra material deposited during the welding procedure. Specimens without welds were also ground using the same procedures.

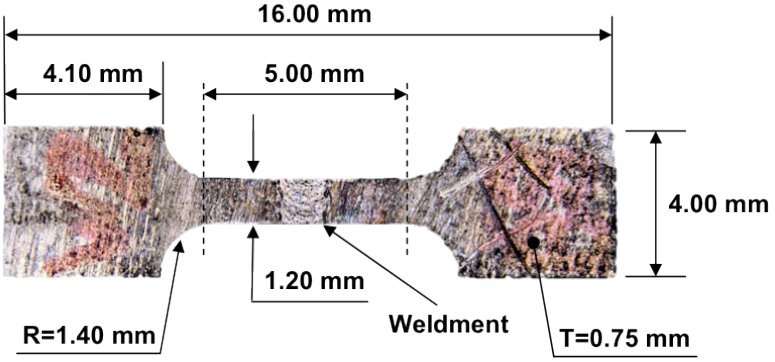

Figure 2: Subsize tensile SS-J3 specimen. Image taken prior to grinding operations.

Tensile tests were performed on a MTS Insight 2-52 one-column tensile screw machine. All tensile tests were performed at room temperature with a strain rate of 0.0011 s^{-1}. Prior to tensile tests, specimens were painted with a random speckle pattern. Several specimens were tested without speckle patterns to characterize deformation relief development. Surface speckle patterns allows for optical, non-contact strain measurements during tensile testing. Strain field measurements were calculated using VIC-2D commercial software and a custom program. The details of digital image correlation (DIC) is presented elsewhere [5, 6]. DIC allows for strain field measurements of base, HAZ, and weld metal on the same tensile specimen. Tensile tests were performed on sub-sized tensile specimens both with and without weldments. Non-welded specimens provided a baseline observation of the mechanical properties of the model alloys.

3. Results and Discussion

3.3 Hardness and Microstructural Analysis

Cross sectional microstructures of the fusion zone, HAZ and base metal for each alloy are shown in Figure 3. The base material (outer regions) has a fine-grained ferrite structure with grain sizes in the range of 20-50 μm for all alloys. The fusion zone demonstrates a distinctly different structure with coarse ferrite grains emanating from the centerline of the weld. The HAZ is difficult to distinguish but recovery and recrystallization is expected due to the heat input from the welding process. Optical investigations in plane and cross section showed no signs of cracking, porosity or other defects within the weldment. Fusion zones had widths on the order of 1-2 mm depending on the specimen and location along the weld traverse.

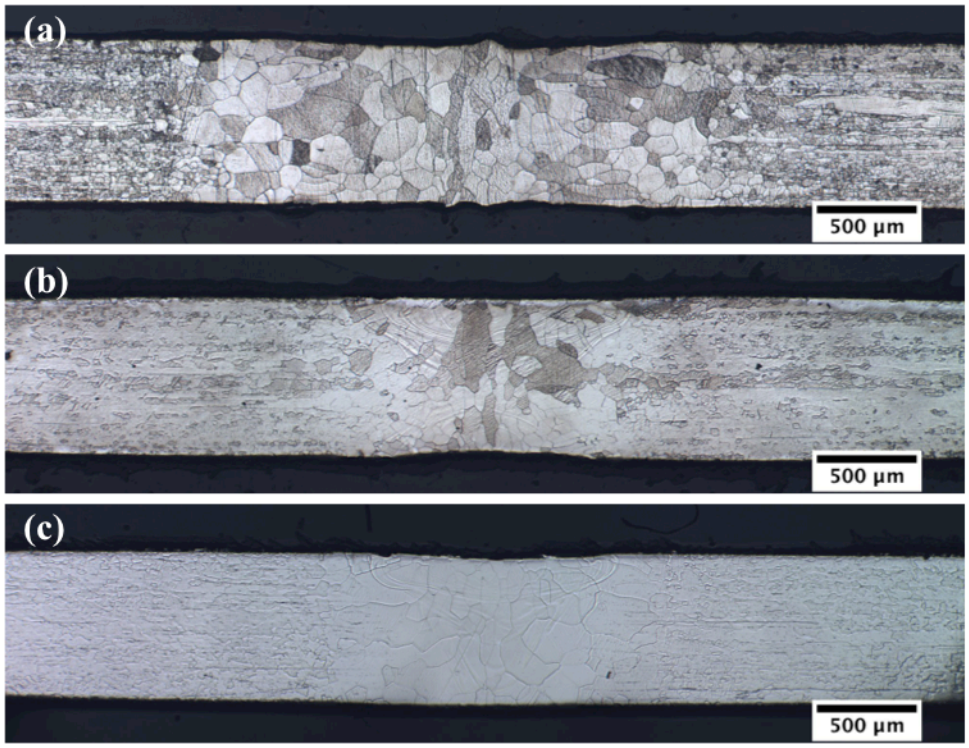

Figure 3: Optical micrographs (images stitched for larger field of view) of fusion zone, HAZ, and base metal for candidate alloys: (a) B125Y, (b) B154Y-2, and (c) B183Y-2.

Cross weld hardness profiles for each alloy are presented in Figure 4. Softening was observed in the weld metal of all alloys with the B183Y-2 showing the highest degree of softening compared to the base metal. Hardness changes were less pronounced in the B125Y or B154Y-2 alloys. The reduction in hardness and change in grain size is summarized for all alloys in Figure 5. This figure shows that the pronounced change in hardness appears to be directly correlated with the change in grain size. Hardness profiles revealed a reduction in hardness about 1-2 mm out from the centerline of the weld. Further analysis is underway to determine if alloying has any effect on the grain size or width of the fusion zone. This reduction in hardness extends further than the apparent width of the fusion zone indicating some loss of cold work within the HAZ. No signs of

embrittlement in the weld, HAZ, or base metal were detected from the hardness traverses.

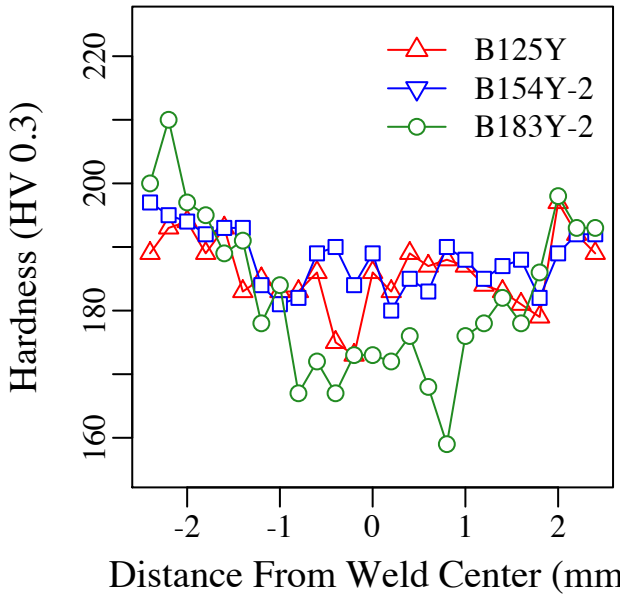

Figure 4: Cross weld hardness profiles for candidate alloys.

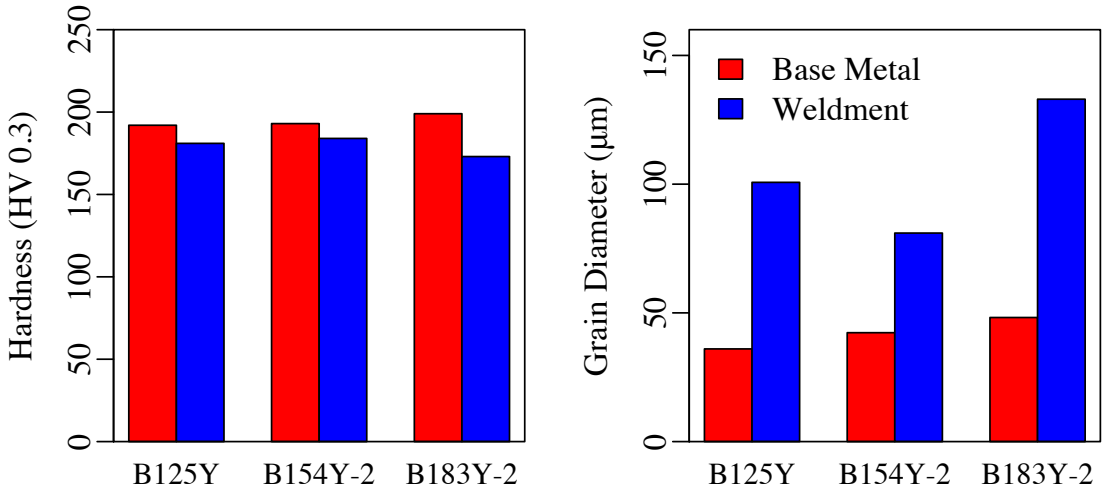

Figure 5: Average microhardness and calculated average grain diameter using linear intercept method.

3.4 Tensile Properties

Figure 6 summarizes the standard tensile properties of yield strength, ultimate tensile strength, uniform elongation, and total elongation for the base metal and fusion zone in the model alloys. The yield strength and ultimate tensile strength of the welded specimens were lower than in the base metal. Welding led to an increase in the uniform elongation but the total elongation changed insignificantly. All three alloys demonstrated similar trends in the tensile properties between the base and weld metal. Initial observations from DIC show that necking and failure occurred within the

fusion zone of all welded specimens. These weldments demonstrated complex behavior due to the gradient of material properties within the gauge region of the tensile specimen. Further analysis is underway to determine the localized strain fields within the welds and to analyze the complex behavior of the weldments under load.

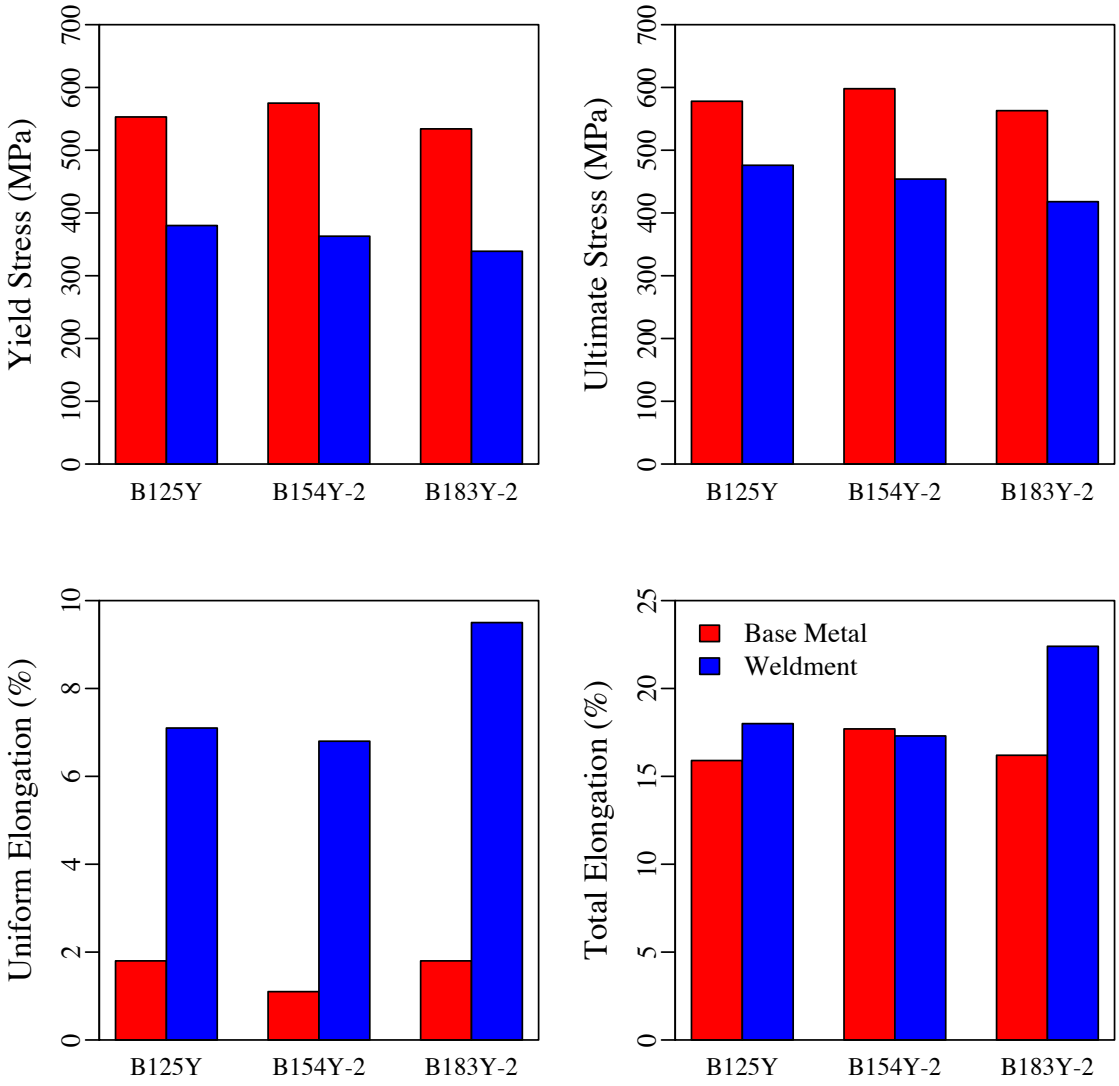

Figure 7: Preliminary values of Yield Stress, Ultimate Stress, Uniform Elongation, and Total Elongation for the base alloy and weldment determined using sub-sized tensile specimens.

4. Summary and Future Work

The weldability of three model FeCrAlY alloys was investigated for thin walled cladding applications. The transverse tensile strength of laser-welded specimens was significantly reduced in the model alloys. Fusion zones exhibited softening and coarse grain structures; however, no embrittlement was observed and all alloys demonstrated ductile behavior and high local ductility. The HAZ zone showed a loss of cold work due to localized heating. Necking in tensile tests occurred within the fusion zone of welded specimens. Welding increased the uniform elongation within the weldment but no significant

increase in total elongation was observed. Further analysis using DIC is being performed to evaluate the deformation localization in the weldments and determine true stress, strain curves for each model alloy.

5. References

1. Rudling, Peter, Alfred Strasser, Friedrich Garzarolli, and Leo van Swam, IZNA7 special topic report: Welding of Zirconium Alloys (2007).
2. K.A. Terrani, S.J. Zinkle, L.L. Snead, Journal of Nuclear Materials (2013).
3. B.A. Pint, K.A. Terrani, M.P. Brady, T. Cheng, J.R. Keiser, Journal of Nuclear Materials in press (2013).
4. M. Moalem, D.R. Olander, Journal of Nuclear Materials 182 (1991) 170.
5. K. Suzuki, S. Jitsukawa, N. Okubo, F. Takada, J.Nucl.Eng. and Design 240 (2010) 1290–1305.
6. B. Pan, K. Qian, H. Xie, A. Asundi, Measurement Science and Technology, 20 (2009) 1–17.